Agricultural Water Management 246 (2021) 106702

Contents lists available at ScienceDirect

Agricultural Water Management

journal homepage: www.elsevier.com/locate/agwat

Effect of root-zone vertical soil moisture heterogeneity on water transport safety in soil-plant-atmosphere continuum in *Robinia pseudoacacia*

Zhongdian Zhang [b,c], Mingbin Huang [a,d,*]

[a] The State Key Laboratory of Soil Erosion and Dryland Farming on the Loess Plateau, Institute of Soil and Water Conservation, Northwest A&F University, Yangling, Shaanxi 712100, China
[b] School of Geographic Sciences, Xinyang Normal University, Xinyang 464000, China
[c] Henan Key Laboratory for Synergistic Prevention of Water and Soil Environmental Pollution, Xinyang Normal University, Xinyang 464000, China
[d] CAS Center for Excellence in Quaternary Science and Global Change, Xian, Shaanxi 710061, China

ARTICLE INFO

Handling Editor - Dr. B.E. Clothier

Keywords:
Soil moisture heterogeneity
Water transport safety
Soil-plant-atmosphere continuum
Plant hydraulic model

ABSTRACT

Soil moisture in root zone is highly heterogeneous in space, while its effect on water transport safety in soil-plant-atmosphere continuum (SPAC) remains poorly understood. In this study, we conducted vertical spilt-root experiments in *R. pseudoacacia* using loamy clay and sandy loam soils in greenhouse, and measured the dynamics of midday transpiration rate, predawn and midday leaf water potential with the lower root zone remaining drought and the upper root zone undergoing the drought-rewatered-drought process. The plant supply-demand hydraulic model was calibrated with the measured data, indicating that the model could efficiently simulate SPAC water transport in *R. pseudoacacia* under the condition of vertical soil moisture heterogeneity. On this basis, we set various combinations of soil moisture in the upper and lower root zones under different soil types and atmospheric evaporative demands in the model, and simulated the variations of indicators describing water transport safety in SPAC, including actual transpiration rate (E), the critical leaf transpiration rate at hydraulic failure (E_{crit}), hydraulic safety margin (HSM), and percentage loss of soil-plant hydraulic conductance (PLK). The numerical simulations suggested that the water transport safety in SPAC varied substantially with vertical soil moisture heterogeneity, and the responses were impacted by soil types and atmospheric evaporative demand. With decreasing soil moisture in the upper root zone (SMC_{up}), E_{crit}, E and HSM remained steady at first and then decreased rapidly when SMC_{up} below a threshold, while PLK exhibited an opposite trend. With decreasing soil moisture in the lower root-zone (SMC_{down}), the curves of E_{crit}, E and HSM presented a descending trend, while the curve of PLK went up. Water transport safety in SPAC declined with decreasing SWC_{up} and SWC_{down} and became more sensitive to SWC_{up} with a lower SWC_{down}. SWC_{down} had greater impact on water transport safety in SPAC under coarser-textured soil with higher atmospheric evaporative demand. The results were supplemental to the traditional analysis of soil water availability to plants under homogeneous condition, and would be helpful for analyzing functional difference of water storage in different soil depths as well as for optimizing water resource management.

1. Introduction

The distribution of soil moisture in root zone varies strongly in time and space (Jia et al., 2016; Ryel et al., 2008; Xi et al., 2013), which results in a marked impact on water transport in soil-plant-atmosphere continuum (SPAC) and other physiological metabolisms, including nutrient uptake, photosynthetic assimilation, etc. (Reich et al., 2018; Sperry and Love, 2015; Yang et al., 2017). In arid and semi-arid area, rooting depths of shrubs and trees usually exceed infiltration depth for precipitation (Fan et al., 2017; Schenk, 2005). Soil moisture in shallow root zone fluctuates rapidly and extremely due to infiltration, soil evaporation and root water uptake. However, soil moisture in deeper root zone changes relatively more slowly with fewer roots and recharge events, resulting in a pronounced vertical soil moisture heterogeneity in root-zone (Fan et al., 2017; Xi et al., 2018a). In agricultural ecosystems, some irrigation techniques including drip irrigation, vertical partial

* Corresponding author at: The State Key laboratory of Soil Erosion and Dryland Farming on the Loess Plateau, Institute of Soil and Water Conservation, Northwest A&F University, Yangling, Shaanxi 712100, China
E-mail address: hmbd@nwsuaf.edu.cn (M. Huang).

https://doi.org/10.1016/j.agwat.2020.106702
Received 23 July 2020; Received in revised form 11 December 2020; Accepted 13 December 2020
Available online 24 December 2020
0378-3774/

root-zone drying method, etc. could also induce vertical soil moisture heterogeneity in root zone for regulating plant water use and enhancing water use efficiency (Ma et al., 2013; Shu et al., 2020; Xi et al., 2016). Although plant response to soil water availability has been studied for decades, most of the studies were under homogeneous soil moisture conditions (Wu et al., 2011c; Yan et al., 2017). Effect of root-zone soil moisture heterogeneity on plant eco-physiological functions is still poorly understood despite its potential importance (Fan et al., 2017; Puértolas et al., 2020; Xi et al., 2018b).

Recently, the response of plant water use to soil moisture heterogeneity has been studied with control experiments (Puértolas et al., 2020), field observations (Gaines et al., 2016), isotopic tracing method (Yang et al., 2015), and numerical modeling (Xi et al., 2016). Accordingly, plants can respond to soil moisture heterogeneity rapidly through hydraulic signals (including leaf water potential, hydraulic conductance, etc.) and chemical signals (including abscisic acid, peptide, etc.) (Huber et al., 2015; Reich et al., 2018; Takahashi et al., 2018). Huber et al. (2015) proposed a mechanistic soil-root water flow model: R-SWMS, and examined the roles of hydraulic and chemical signals in regulating leaf water potential and transpiration under horizontal and vertical soil moisture heterogeneity in root zone. Their results supported that isohydric plant behavior originates from the combined control of hydraulic and chemical signals whereas anisohydric behavior emerges mainly from the control of chemical signals. Recent reports suggested that roots of some species can move water from moist to dry soil through hydraulic redistribution (Neumann and Cardon, 2012; Prieto et al., 2012), which can increase dry-season transpiration and photosynthetic rates (Domec et al., 2010), prolong the life span of fine roots (Bauerle et al., 2008), and maintain root-soil contact in dry soils (Caldwell et al., 1998; Domec et al., 2004). Hydraulic redistribution helps plants present as an efficient adaptability to heterogeneous soil moisture. Based on the physiological mechanism and experimental findings, Ryel et al. (2008) proposed a conceptual model indicating that a growth pool is located in shallow soil layer and a maintenance pool is in deeper soil layer. Yang et al. (2017) also found that deeper soil water contributes to drought avoidance and shallower soil water determines the growing rate of trees based on long-term field observations.

According to the cohesion–tension theory, transpiration stream is pulled through porous media in soil and xylem conduits of plant. As soil and atmosphere drought progressed, more negative pressures increase flow resistance by causing cavitation in xylem conduits and draining of soil pores in rhizosphere, thus endanger water transport safety in SPAC (Sperry and Love, 2015). Water transport safety in SPAC plays a critical role in determining plant growth and survival during drought stress (Choat et al., 2018; Wolfe et al., 2016). Hence, analyzing the response of water transport safety in SPAC to vertical soil moisture heterogeneity is essential in understanding plant water relationships and helps to optimize water resources management.

Based on previous studies under homogeneous soil moisture conditions (Wu et al., 2011a, 2015), the responses of plant water uptake and loss in SPAC to soil water availability were affected by multiple factors, including soil texture, plant species, atmospheric evaporative demand, etc. Researchers have developed various mathematical models to examine the effect of these factors on the responses of plants to soil water availability (Huber et al., 2015; Novak et al., 2005). In traditional SPAC models, response of root water uptake and canopy transpiration to soil and atmospheric drought was generally described with prescribed empirical stress functions in numerous mathematical forms based on experiments (Damour et al., 2010; Feddes et al., 1978; Gharsallah et al., 2013). The coupling between water uptake and loss in SPAC is loose, and there is a lack of mechanisms for simulating SPAC water transport (Tai et al., 2018). With the development of plant hydraulics, more mechanistic based models were developed for coupling root water uptake and canopy loss in a more direct way (Huber et al., 2015; Sperry and Love, 2015; Sperry et al., 2003). Based on the similarity in soil and xylem water transport in physics, Sperry et al. (1998) developed a resistance-network model to describe water transport in soil-plant system mechanistically. Sperry and Love (2015) further developed the supply-demand theory, and upgraded soil-plant model for simulating SPAC water transport by including the stomatal control of transpiration and leaf water potential (abbreviated as Sperry model). Based on soil water potential profile, vapor pressure deficit (VPD), and hydraulic properties of soil and xylem, Sperry model could directly solve water flux, canopy conductance and the distribution of water potential and hydraulic conductance in SPAC (Sperry and Love, 2015; Sperry et al., 2016). Thus, this model serves as an efficient tool for analyzing the effect of vertical soil moisture heterogeneity on water transport safety in SPAC.

Robinia pseudoacacia L. (black locust) has been widely planted around the world. It plays an essential role in improving environmental quality and reducing soil erosion (Li et al., 2018). In Loess Plateau, *R. pseudoacacia* was commonly chosen as a pioneer afforestation species in revegetation and has been planted on over 10 million hectares of this area (Ma et al., 2017). The groundwater level in the Loess Plateau generally varies from 30 to 100 m below land surface (Jia et al., 2017), and water from precipitation is a sole source for water consumption of *R. pseudoacacia* trees. According to previous studies, rooting depth of *R. pseudoacacia* was generally deeper than 3–5 m (Wang et al., 2011; Zhang et al., 2018), while mean annual infiltration depth ranged between 1 and 2 m (Chen et al., 2008; Hu et al., 2011). It has been widely found that a dry soil layer with low soil moisture content below the infiltration depth was formed after *R. pseudoacacia* trees grew more than eight years (Jia et al., 2019; Wang et al., 2011, 2013). The characteristics of dry soil layer are summarized as: (1) locating at a certain soil depth, mainly between 2 and 10 m below the soil surface (Wang et al., 2013); (2) soil moisture content ranges between permanent wilting point and stable field capacity, which is generally considered to be equivalent to 60% of field capacity (Chen et al., 2008); and (3) spatial and temporal persistence and hardly replenished by rainfall infiltration in a regular year. Dry soil layer has been regarded as a major potential threat to the sustainability of the revegetation project (Jia et al., 2017; Shangguan, 2007; Wang et al., 2020; Zhang et al., 2020). After the formation of dry soil layer, soil moisture fluctuates heavily within infiltration depth but remains at a low level at deeper soil layer. Soil moisture heterogeneity would become more intensive in root zone and further affect SPAC water transport and other physiological properties (Shao et al., 2016; Wei et al., 2018; Xi et al., 2018a). Therefore, characterizing the effect of root-zone vertical soil moisture heterogeneity on water transport safety in SPAC would be helpful for evaluating and improving the sustainability of *R. pseudoacacia* plantations (Jia et al., 2020).

The objectives of this study were to (1) examine the applicability of Sperry model in simulating SPAC water transport under the condition of heterogeneous soil moisture induced by underlying dry soil layer; (2) analyze the effect of heterogeneous soil moisture on water transport safety in SPAC under different environmental conditions using numerical simulations.

2. Materials and methods

2.1. Vertical spilt-root experiments

To evaluate Sperry model for simulating SPAC water transport in *R. pseudoacacia* under the condition of root-zone vertical soil moisture heterogeneity, we conducted vertical split-root experiments with two soil types in greenhouse. The greenhouse was located at Northwest A&F University in Yangling, Shaanxi Province (34.27°N , 108.07°E). This site is characterized as a temperate and semi-humid climate. Mean annual precipitation is 639.8 mm and mean annual temperature is 13.5 °C. The soils used in this study were two major soil types in Loess Plateau: Lou soil (Anthrosol) and Huangmian soil (Calcaric Cambisol). According to the FAO classification system, the texture of Lou soil and

Huangmian soil is loamy clay and sandy loam, respectively. Lou soil was collected from Yangling and Huangmian soil was collected from Mizhi. Then, the soils were passed through a 2-mm sieve to remove any large objects, and packed into the acrylic columns (90 cm high, 23.5 cm in diameter) at a bulk density of 1.35 g cm^{-3} and 1.30 g cm^{-3}, respectively. Physical properties of the two soil types were shown in Table 1. Soil particle sizes were measured using a particle size analyzer, Mastersizer 2000 (Malvern Instruments, Malvern, England). Soil–water retention curves were determined using centrifugation method, and then they were fitted with the van Genuchten model using RETC program (van Genuchten, 1992).

The soil column was divided into upper and lower compartments (40 cm in depth for each compartment) by a 3–4 cm thick quartzite gravel (4–8 mm particle diameter) to prevent water capillarity between two compartments (Fig. 1). Soil surface was covered with 3–4 cm thick quartzite gravel to minimize water loss (Zhou et al., 2016). A hole was punched in the wall of column at the top of lower compartment, and the soil in lower compartment was irrigated by drip irrigation, where water is allowed to drip into soils through the holes from pipe. After the columns were packed, two unbalanced three-rod time domain reflectometry (TDR) probes (Campbell Scientific Inc., Logan, UT, USA) were inserted horizontally into each compartment at 20-cm depth intervals to measure the soil moisture content. Before the experiments were carried out, TDR probes were calibrated using gravimetric method. During the period of experiment, air circulation between the greenhouse and outside was facilitated by the window at roof and axial flow fan equipped at the side wall of greenhouse. The dynamics of air temperature, relative humidity, and vapor pressure deficit during the experimental period were shown in Fig. 2. Field capacity (FC) was determined using the modified Wilcox method (Hanks et al., 1954). Permanent wilting point was determined by growing and wilting *R. pseudoacacia* seedlings in each of the two soils (Wu et al., 2015).

In semi-arid and arid areas like Loess Plateau, soil moisture within infiltration depth fluctuates heavily due to rainfall events and evapotranspiration. While soil moisture at the deeper soil cannot be recharged and stay at low moisture value after the formation of a dry soil layer in *R. pseudoacacia* stands. According to the soil moisture profile characteristics under natural conditions, we designed a drought-rewatered-drought treatment at the upper compartment and the lower compartment was withheld water since 60%FC in this study. In mid-March 2019, 20 two-year-old *R. pseudoacacia* seedlings with similar growing status were transplanted from field to soil columns for seedling cultivation. There were 10 plants in each soil type. All plants were well watered to maintain 80–100%FC at both the upper and lower compartments for two months to allow natural establishment. Then 4 plants with similar whole plant leaf area in each soil type were chosen for subsequent experiments. This method could decrease the experimental errors resulting from the difference in individual plants. These plants were

Table 1
Soil physical properties of Lou soil and Huangmian soil.

	Lou	Huangmian
Texture	Loamy clay	Sandy loam
Bulk density (g cm^{-3})	1.35	1.30
Soil particle composition		
Sand content (%)	32.2	11.7
Silt content (%)	36.6	16.3
Clay content (%)	31.2	72.0
Parameters of van Genuchten		
θ_r (cm^3 cm^{-3})	0.048	0.000
θ_s (cm^3 cm^{-3})	0.463	0.426
α (cm^{-1})	0.01078	0.07041
n	1.592	1.135
Field capacity (cm^3 cm^{-3})	0.283	0.224
Permanent wilting point (cm^3 cm^{-3})	0.147	0.061

Note: θ_r, residual volumetric water content, θ_s, saturated volumetric water content.

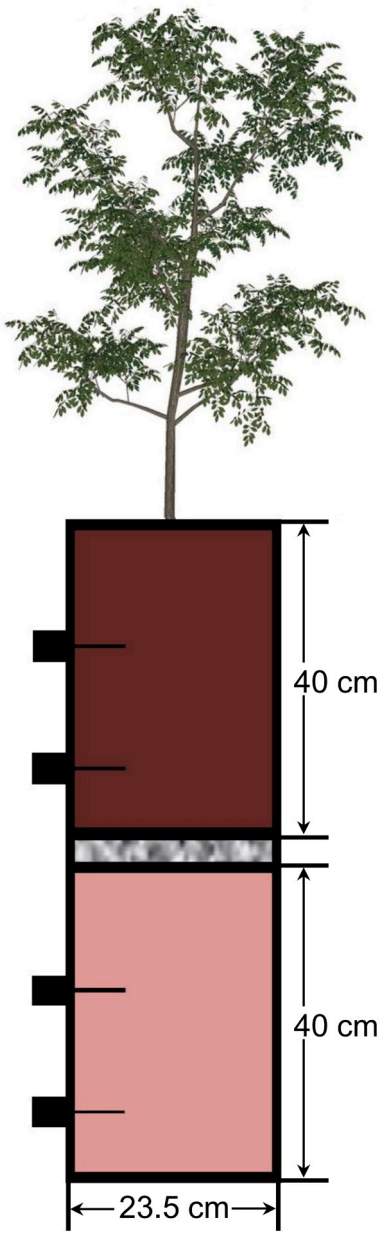

Fig. 1. Schematic representation of the vertical spilt-root experiment.

138.3 ± 5.8 cm in height, 12.0 ± 0.5 mm in basal diameter and 6247.7 ± 328.7 cm^2 in whole plant leaf area at the start of the experiment. Before the experiment, both the upper and lower compartments were withheld water until the soil moisture content decreased to 60%FC, then the upper compartment was irrigated to field capacity and then withheld water to start the first drought. When predawn leaf water potential decreased to −2.5∼−2 MPa, the upper compartment was rewatered to field capacity and then the second drought started (Fig. 3).

During the experiment, soil moisture content at the upper and lower compartment was measured daily with TDR. Predawn and midday leaf water potentials were measured daily using pressure chamber (PMS Instrument Co., Corvallis, OR, USA) at 5:00–6:00 and 13:00–14:00, respectively. The length (LL, cm) and width (LW, cm) of newly produced leaves were measured daily, and incremental leaf area (LA, cm^2) was calculated with an empirical equation developed by Zhang et al. (2019). Detached leaves for measuring leaf water potential and deciduous leaves were also collected, scanned with a digital scanner (Canon LiDE 120, Canon Inc., Tokyo, Japan), and leaf area was measured using an image

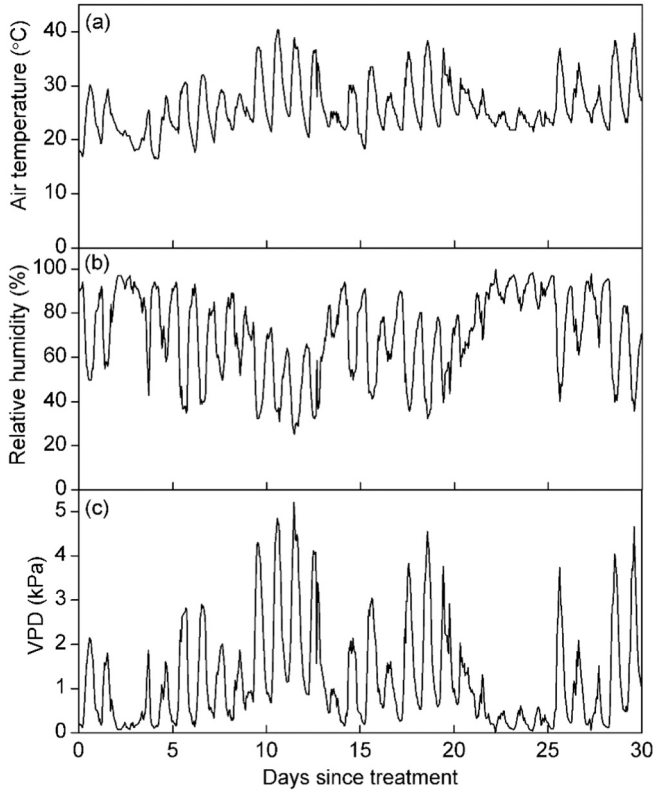

Fig. 2. Time courses of air temperature (a), relative humidity (b) and vapor pressure deficit (VPD, c) during the experimental period.

processing program, ImageJ (http://rsbweb.nih.gov/ij/index.html). At the end of the experiment, all leaves were harvested and scanned, and whole plant leaf area was measured using ImageJ. Therefore, the dynamics of whole plant leaf area during the period of the experiment could be calculated based on final leaf area, daily incremental and losing leaf area during the experiment. Sap flow was measured using Flow32–1 K system (Dynamax. Inc., Houston, Texas, USA). Gauge output was monitored every 60 s and recorded as 15-min averages with a CR1000 data logger (Campbell Scientific, Logan, UT, USA). Leaf transpiration rate was calculated by dividing sap flow by whole plant leaf area. After the experiment, current-year shoots were collected and xylem vulnerability curve was measured using the bench top dehydration method (Sperry et al., 1988; Wang et al., 2014), and further fitted with Weibull function:

$$PLC = 1 - e^{-\left(-\Psi_{xylem}/b\right)^c} \quad (1)$$

where PLC is the percentage loss of xylem hydraulic conductivity; Ψ_{xylem} is xylem water potential; and b and c are fitted parameters. Roots were separated from soil by flushing through a fine mesh bag (60 mesh). Fine roots (diameter <2 mm) were dried at 65 °C to constant mass, and fine root biomass at upper and lower compartment was then determined (Fig. S1).

2.2. Sperry model

The Sperry model is a trait-based soil-plant-atmosphere model (Sperry et al., 2016) which solves water flux, water potential and hydraulic conductance in SPAC at a given soil water potential profile and vapor pressure deficit. Complete details in Sperry model can be found in previous literatures (Sperry and Love, 2015; Sperry et al., 2016), and a brief summary of relevant equations is provided here. The SPAC system is divided into leaf, stem, root, and rhizosphere components in series. The steady-state flow rate through each component, E_i, can be calculated by the integral transform of the component's vulnerability curve ($k(\Psi)_i$):

$$E_i = \int_{\Psi_{down}}^{\Psi_{up}} k(\Psi)_i d\Psi \quad (2)$$

where $k(\Psi)_i$ quantifies the decline of hydraulic conductance (k) with decreasing water potential (Ψ) for each component. k decreases with decreasing Ψ due to cavitation for xylem components, which can be quantified using a two-parameter Weibull function (b and c):

$$k_i = k_{x,\,max} e^{-\left(-\Psi_x/b\right)^c} \quad (3)$$

where $k_{x,max}$ is the maximum hydraulic conductance and Ψ_x is water potential of xylem components including leaf, stem and root. In rhizosphere components, the decrease of k with decreasing Ψ is caused by the displacement of water-filled pore space by air as capillary forces fail, which can be described using a van Genuchten function (van Genuchten, 1980):

$$k_i = k_{s,\,max} v^{(n-1)/2n}\left[(1-v)^{(n-1)/n} - 1\right]^2 \quad (4)$$

$$v = \left[(\alpha\Psi_{soil})^n + 1\right]^{-1} \quad (5)$$

where $k_{s,max}$ is the maximum hydraulic conductance of rhizosphere components and n and α are texture-specific parameters.

The $E(\Psi_{leaf})$ supply function is calculated by solving leaf water potential (Ψ_{leaf}) as transpiration rate (E) increases from zero for the entire continuum. Increasing E is associated with decreases in Ψ_{leaf} and soil-plant hydraulic conductance (k_p). Mathematically, E reaches a maximum, E_{crit}, as k_p approached zero and Ψ_{leaf} decreased to the corresponding minimum value (Ψ_{crit}), which results in hydraulic failure in SPAC and thus plant cannot transport water (Sperry et al., 1998; Sperry

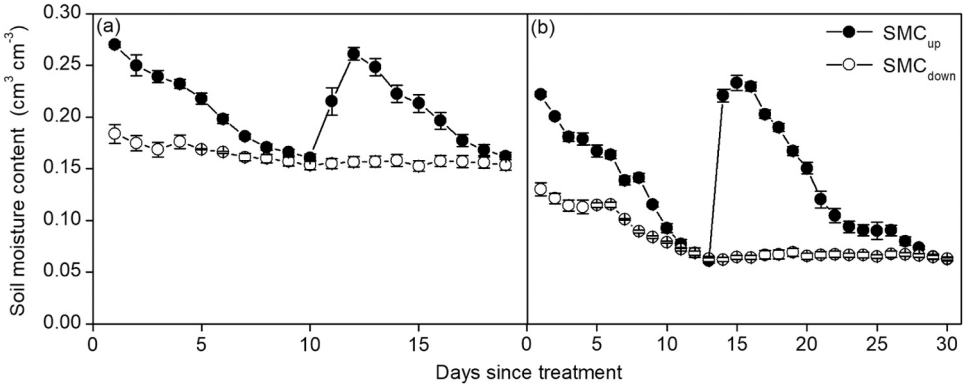

Fig. 3. Time courses of soil moisture content at upper compartment (SMC_{up}) and soil moisture content at lower compartment (SMC_{down}) of loamy clay (a) and sandy loam (b) columns. Bars indicate ± SE, $n = 4$.

and Love, 2015).

As supposed by the supply-demand theory, canopy water demand is regulated in proportion to threat to supply posed by xylem cavitation and soil drying. Stomata are assumed to regulate the pressure drop between soil and leaf water potential ($\Delta\Psi$) based on the fractional drop in soil-plant hydraulic conductance from its maximum:

$$\Delta\Psi = \Delta\Psi'\left[\left(dE'/d\Psi_{leaf}\right)/\left(dE/d\Psi_{max}\right)\right] \quad (6)$$

where $\Delta\Psi'$ is the unregulated pressure drop that is derived from supply function with unregulated transpiration rate: E'=VPD×G_{max}, where G_{max} is maximum diffusive conductance. Therefore, the regulated transpiration rate is given by $\Delta\Psi$ based on supply function. Root zone can be divided into multiple layers, and each layer includes root and rhizosphere components. Maximum conductance values of root and rhizosphere were determined based on the proportions of root and rhizosphere resistances in the soil-root system, and they were partitioned into each layer according to fine root distribution. The actual conductance of root and rhizosphere in each layer can be calculated based on the vulnerability curves. Root water uptake rate in each layer can be solved using the multidimensional Newton-Raphson method (Sperry et al., 2016).

In the vertical spilt-root experiment, the distribution of fine root biomass was nearly homogeneous in the soil column (Fig. S1). We divided the root and rhizosphere components into 2 compartments with equal roots in the modeling study. The depth of each layer was set to be 40 cm as per the vertical spilt-root experiment. The parameters of VC were assumed to be the same for leaf, stem, and root. Maximum soil-plant hydraulic conductance (k_{max}), G_{max}, and average percentage of rhizosphere resistance in whole soil-plant hydraulic resistance (P_{rhiz}) are difficult to measure directly, and are optimized by fitting the model to observed data (Sperry et al., 2016; Tai et al., 2018). As suggested by Sperry et al. (2016), we estimated the parameters with the downhill simplex algorithm based on measured midday leaf transpiration rate (E_{md}) and midday leaf water potential (Ψ_{md}) in the experiments. Each value was 'studentized' by subtracting the respective measurement mean and dividing by the standard deviation to equalize weighting across E_{md} and Ψ_{md}. The absolute error averaged across the studentized E_{md} and Ψ_{md} was minimized by adjusting k_{max}, G_{max} and P_{rhiz} with the downhill simplex algorithm to ensure global minimums to be obtained (Nelder and Mead, 1965; Sperry et al., 2016). According to the sensitivity analysis conducted by Sperry et al. (2016), the outputted E_{md} is sensitivity to k_{max} and G_{max}, while Ψ_{md} is sensitivity to k_{max}, G_{max} and P_{rhiz}. Major parameters and values used in this study are summarized in Table 2. The hydraulic conductance was expressed per leaf area in this study to eliminate the difference of whole plant leaf area among individual plants (Sperry et al., 1998).

2.3. Indicators of water transport safety and their responses to soil moisture heterogeneity

E, E_{crit}, hydraulic safety margin (HSM) and the percentage loss of soil-plant hydraulic conductance (PLK) were used as indicators to describe water transport safety in SPAC (Sperry et al., 1998; Sperry and Love, 2015; Tai et al., 2017, 2018). HSM is defined as the difference between E_{crit} and E (Sperry et al., 1998). E_{crit} was determined via an iteration algorithm as k_p approached zero ($< k_{max}/2000$ as defined in the model), which enabled the estimated error of E_{crit} less than 0.01 mmol m^{-2} s^{-1} (Sperry et al., 1998, 2016). PLK was calculated by:

$$PLK = 1 - \frac{k_p}{k_{max}} \quad (7)$$

Obviously, water transport safety in SPAC would be worse with increasing E and PLK, and decreasing E_{crit} and HSM.

The indicators including E_{crit}, HSM, and PLK are difficult to measure directly, which are only estimated by plant hydraulic model (Choat et al., 2018; Sperry et al., 2016). Therefore, we focused on the model analysis in this study. To quantify the response of water transport safety in SPAC to root-zone vertical soil moisture heterogeneity, we set a series of soil moisture contents at the upper and lower compartments in Sperry model, and examined the changes of E, E_{crit}, HSM and PLK with different soil water combinations at upper and lower compartments. Soil types were loamy clay and sandy loam. The simulated soil moisture contents in upper and lower compartments were in the range of permanent wilting point and field capacity (Table 1), which is 0.15–0.28 cm^3 cm^{-3} for loamy clay and 0.06–0.22 cm^3 cm^{-3} for sandy loam at the interval of 0.01 cm^3 cm^{-3}, respectively. We also set different VPD to assess the effect of atmospheric factors on the response of water transport safety in SPAC to soil moisture heterogeneity. Three levels of VPD were set as: 1.5 kPa (low), 3.0 kPa (middle) and 4.5 kPa (high), reflecting different atmospheric evaporate demand.

Table 2
The parameters and values of Sperry model.

Parameter	Value
Weibull function b and c for root, stem, leaf	b = 2.5, c = 4.3
Maximum soil-plant hydraulic conductance per leaf area (k_{max}, mmol m^{-2} s^{-1} MPa^{-1})	2.4
Maximum diffusive conductance to water vapor (G_{max}, mmol m^{-2} s^{-1})	94.8
Average percentage of rhizosphere resistance in whole soil-plant hydraulic resistance (P_{rhiz}, %)	20
Number of root and soil layers	2

2.4. Statistical analysis

The performance of Sperry model was evaluated with the coefficient of determination (R^2) and root mean square error (RMSE). RMSE was calculated using the following equation:

$$RMSE = \sqrt{\frac{1}{n}\sum_{i=1}^{n}(O_i - P_i)^2} \quad (8)$$

where O_i and P_i are observed and predicted values, respectively. In loam clay and sandy loam, RMSE and R^2 of each parameter were calculated based on 19 and 30 pairs of observed and predicted values, respectively.

In numerical simulations, we plotted the variation in E, E_{crit}, HSM and PLK with changing soil moisture content in upper layer (SMC_{up}) under different soil moisture content in lower layer (SMC_{down}). We mainly focused on the minimum, maximum and threshold values of different curves. We fitted each curve with the Logistic function:

$$y = c_1 + \frac{c_2}{1 + \exp\left(\frac{SMC_{up} + c_3}{c_4}\right)} \quad (9)$$

where y is the regressed indicator, c_1, c_2, c_3 and c_4 are fitted parameters. Based on the regressed equations, we calculated the threshold value of SMC_{up} for each indicator using the method of Yan et al. (2017). The threshold is defined as the corresponding SMC_{up} when the change of regressed indicator is greater than 5% of the difference between the maximum and minimum value as SMC_{up} decreases from field capacity.

3. Results

3.1. Model evaluation

The temporal variations in soil moisture content at upper and lower compartments are shown in Fig. 3. The experiment lasted for 19 d and 30 d in loamy clay and sandy loam soil, respectively. During the first drought, SMC_{up} decreased quickly from field capacity before rewetting,

and SMC_{down} exhibited a slow decrease from 60%FC at the same time. The SMC_{up} and SMC_{down} reached similar values before rewetting, which was 0.154 cm^3 cm^{-3} and 0.066 cm^3 cm^{-3} for loamy clay and sandy loam, respectively. In both soil types, SMC_{up} recovered to field capacity after rewetting and then decreased with time, while SMC_{down} remained relatively stable during the second drought.

The Sperry model could well simulate the temporal variation in predawn leaf water potential (Ψ_{pd}), midday leaf water potential (Ψ_{md}) and midday leaf transpiration rate (E_{md}) during the experimental period (Fig. 4). During the first and second drought periods, Ψ_{pd} varied between −0.3∼−0.2 MPa in the early period and then decreased quickly (Fig. 4b, e). In loam clay, the RMSE and R^2 between observed and simulated E_{md} were 0.388 mmol m^{-2} s^{-1} and 0.939, respectively. The RMSE and R^2 were 0.223 MPa and 0.915 for Ψ_{pd}, 0.352 MPa and 0.892 for Ψ_{md}, respectively. There was larger variation between the simulated and observed values in sandy loam. The prediction in sandy loam was slightly worse than that of the loamy clay. The RMSE and R^2 were 0.461 mmol m^{-2} s^{-1} and 0.702 for E_{md}, 0.325 MPa and 0.880 for Ψ_{pd}, 0.373 MPa and 0.832 for Ψ_{md}, respectively.

3.2. Responses of water transport safety to soil moisture heterogeneity

Under natural conditions, the soil moisture content generally changed rapidly in shallow soil and was relatively stable in the deeper soil layer. So the responses of the four indicators to different combinations of SMC_{up} and SMC_{down} were simulated using the calibrated Sperry model, and the effects of VPD and soil textures on the indicators were analyzed. With the same SMC_{down} values, there was little changes in E, E_{crit} and SME when SMC_{up} was higher than the thresholds, then they decreased rapidly with decreasing SMC_{up}, presenting as s-shape curves (Figs. 5–7). On the contrary, PLK exhibited a rapid increase when SMC_{up} was lower than the thresholds (Fig. 8). All indicators had similar patterns in loamy clay and sandy loam soils. As SMC_{down} decreased from field capacity to permanent wilting point, the maximum and minimum values of the curves were in the similar ranges for different soil types. Compared with loamy clay, the threshold was lower and the indicators changed faster in sandy loam when SMC_{up} decreased below the threshold. The combinations of soil moisture in upper and lower layers contained a series of homogeneous conditions from wet to dry. For the simulations of E, E_{crit} and HSM, the maximum soil moisture value was under the condition of homogeneous field capacity in root zone, the minimum soil moisture value was under the condition of homogeneous permanent wilting point in root zone in each soil type with different atmosphere evaporative demands. PLK presented opposite trend.

3.2.1. Change of the E-SMC_{up} curve with SMC_{down}

The E-SMC_{up} curve showed a descending trend with decreasing SMC_{down} (Fig. 5), and the change of the E-SMC_{up} curve with SMC_{down}

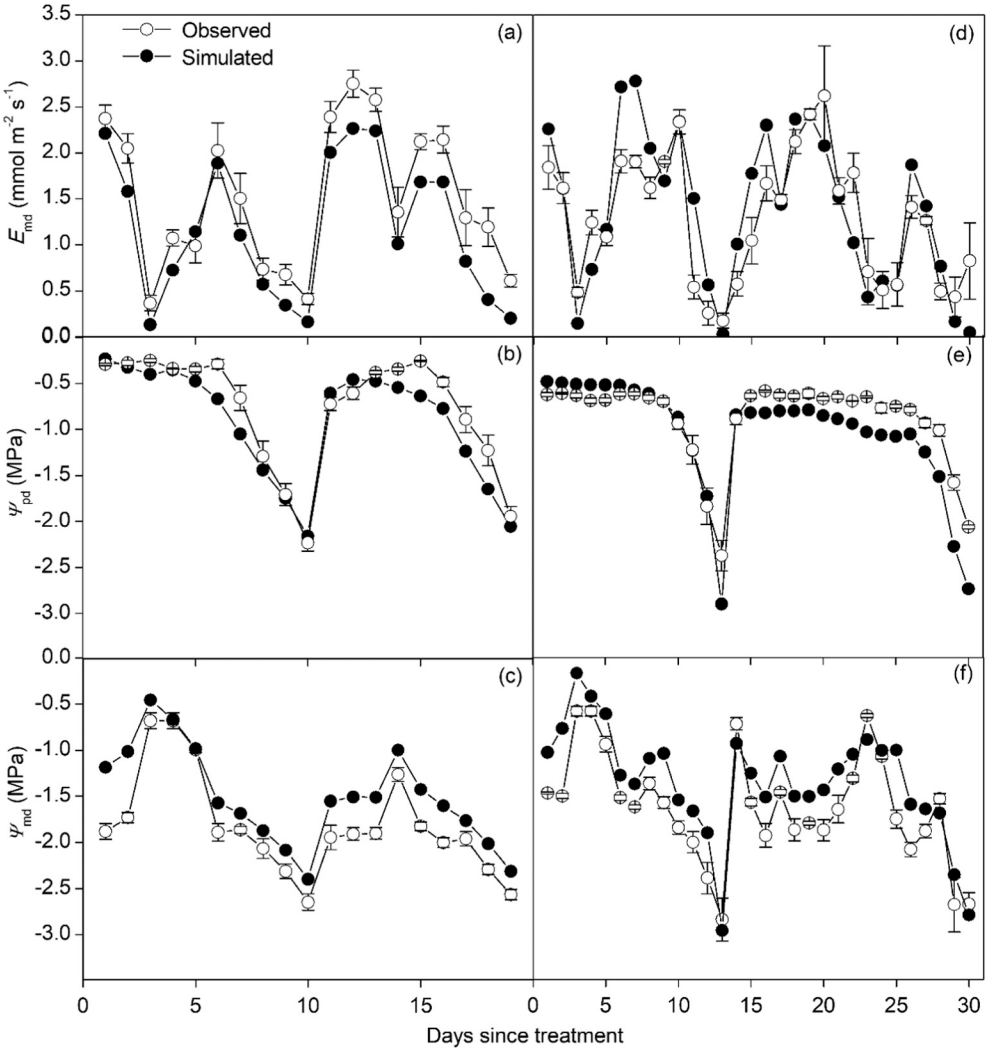

Fig. 4. Comparison between simulated and observed midday leaf transpiration rate (E_{md}), predawn leaf water potential (Ψ_{pd}) and midday leaf water potential (Ψ_{md}) in loamy clay (a∼c) and sandy loam (d∼f). Bars indicate ± SE, $n = 4$.

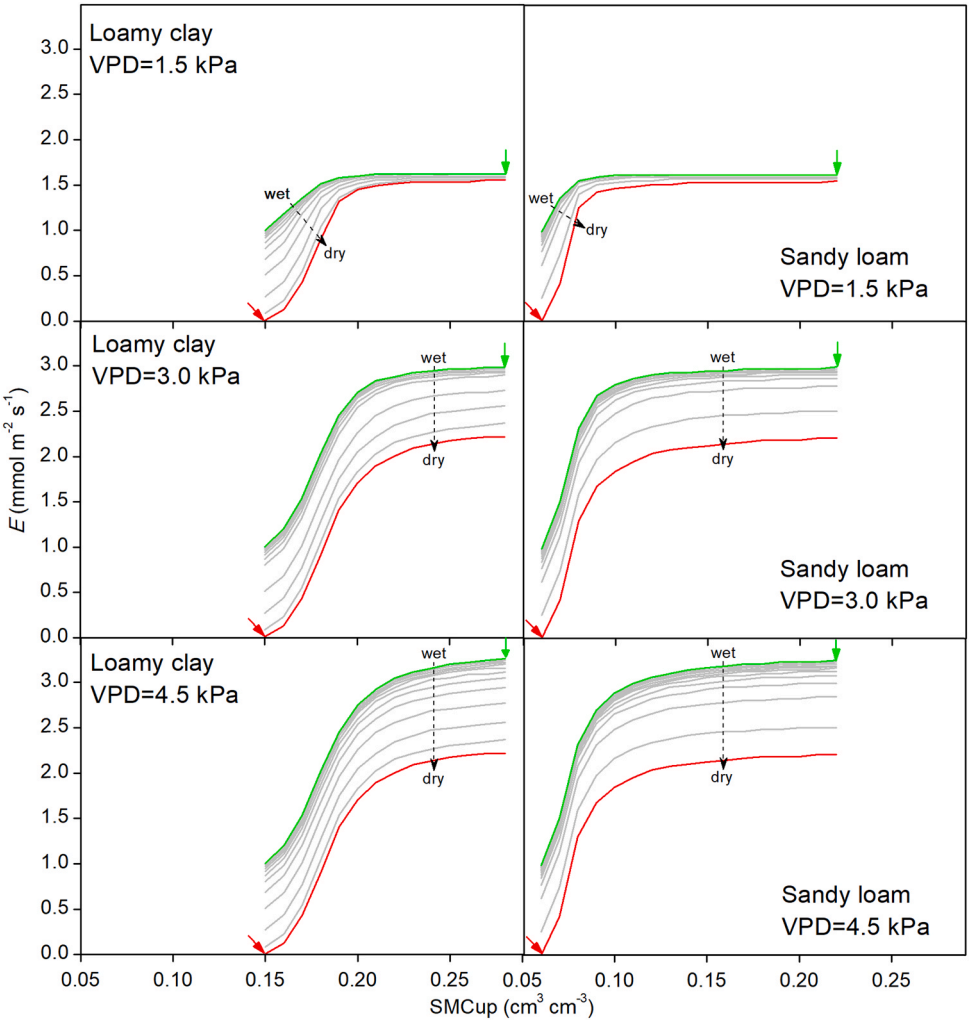

Fig. 5. Responses of leaf transpiration rate (E) to root-zone vertical soil moisture heterogeneity. Soil moisture contents at upper compartment (SMC_{up}) and lower compartment were in the range of permanent wilting point and field capacity, which was 0.15–0.28 cm^3 cm^{-3} for loamy clay and 0.06–0.22 cm^3 cm^{-3} for sandy loam at the interval of 0.01 cm^3 cm^{-3}, respectively. The lines represent SMC_{up}-E curves under different soil moisture content at lower compartment. The top and bottom curves represent field capacity and permanent wilting point at lower compartment, respectively. The right and left arrows point to the condition of homogeneous field capacity and permanent wilting point in root zone, respectively.

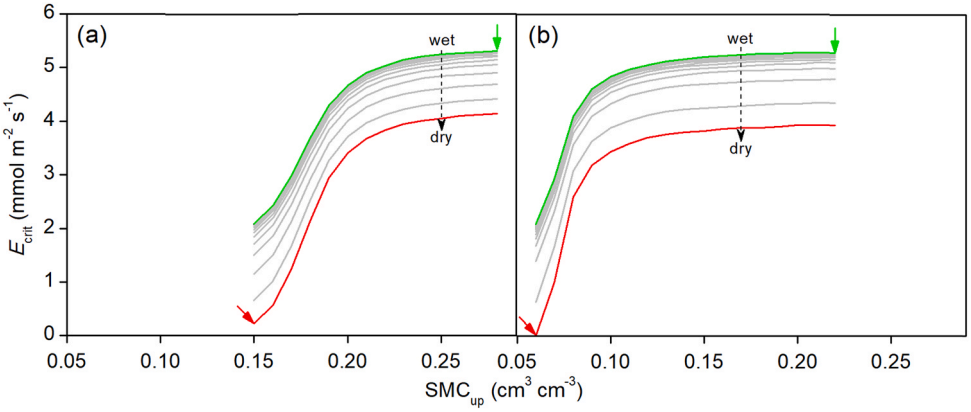

Fig. 6. Responses of critical leaf transpiration rate at hydraulic failure (E_{crit}) to root-zone vertical soil moisture heterogeneity. Soil moisture contents at the upper compartment (SMC_{up}) and the lower compartment were in the range of permanent wilting point and field capacity, which was 0.15–0.28 cm^3 cm^{-3} for loamy clay (a) and 0.06–0.22 cm^3 cm^{-3} for sandy loam (b) at the interval of 0.01 cm^3 cm^{-3}, respectively. The lines represent SMC_{up}-E_{crit} curves under different soil moisture content at the lower compartment. The top and bottom curves represent field capacity and permanent wilting point at lower compartment, respectively. The right and left arrows point to the condition of homogeneous field capacity and permanent wilting point in root zone, respectively.

exhibited different patterns under different VPD. Under low VPD, the threshold was similar among different curves, ranged between 0.193 and 0.202 cm^3 cm^{-3} for loamy clay and 0.085–0.087 cm^3 cm^{-3} for sandy loam. As SMC_{down} decreased from field capacity to permanent wilting point, the maximum value slightly differed among different curves (1.5–1.6 mmol m^{-2} s^{-1}), while E dropped faster when SMC_{up} decreased below the threshold, and the minimum value dropped from 1.01 to 0.01 mmol m^{-2} s^{-1} in the two soil types.

Under middle VPD, the threshold increased from 0.209 to 0.227 mmol m^{-2} s^{-1} for loamy clay and from 0.101 to 0.116 cm^3 cm^{-3} for sandy loam as SMC_{down} decreased from field capacity to permanent wilting point. The maximum value decreased from 2.99 to 2.22 mmol m^{-2} s^{-1}, E decreased in similar rates when SMC_{up} decreased below the threshold, and the minimum value decreased from 1.01 to 0.01 mmol m^{-2} s^{-1} with decreasing SMC_{down}.

Under high VPD, the threshold differed little among different curves.

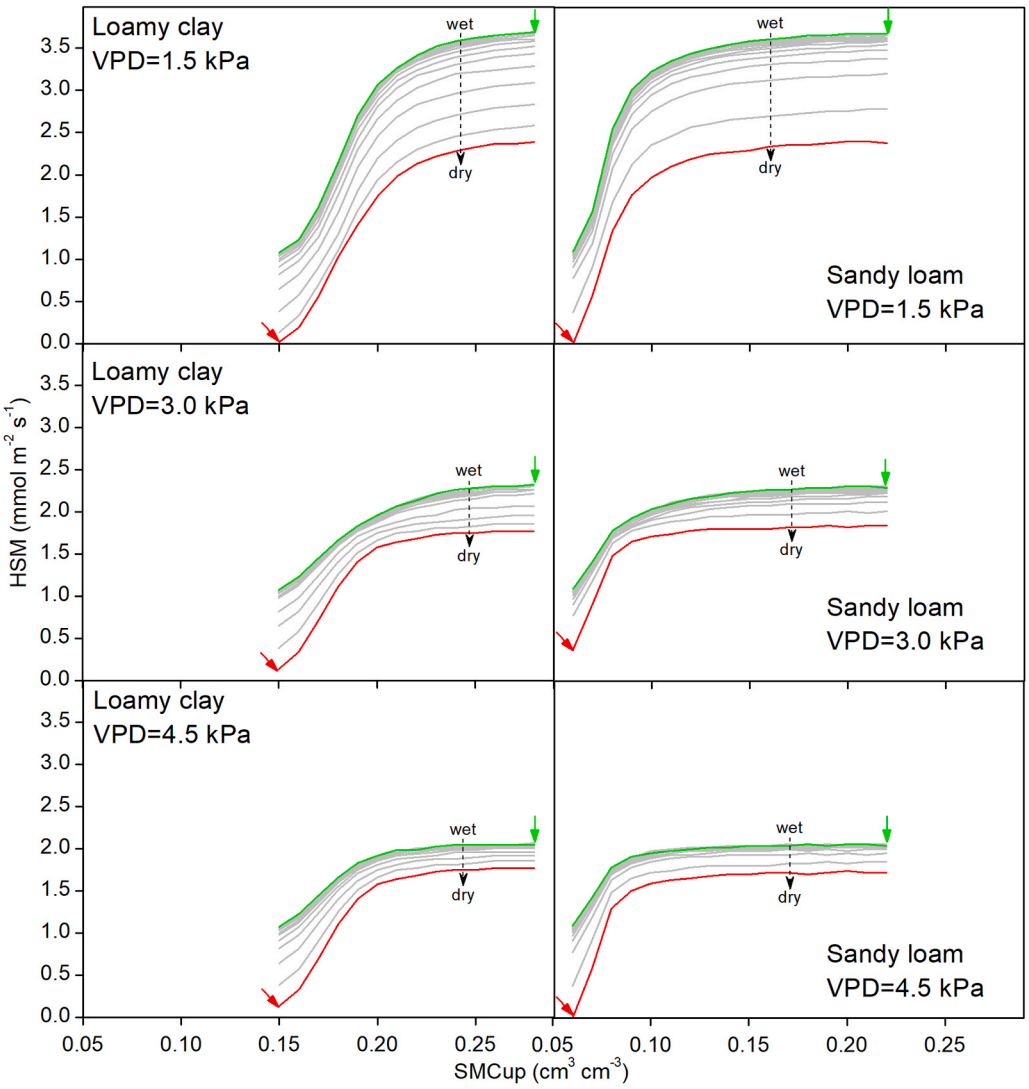

Fig. 7. Responses of hydraulic safety margin (HSM) to root-zone vertical soil moisture heterogeneity. Soil moisture contents at upper compartment (SMC_{up}) and lower compartment were in the range of permanent wilting point and field capacity, which was 0.15–0.28 cm^3 cm^{-3} for loamy clay and 0.06–0.22 cm^3 cm^{-3} for sandy loam at the interval of 0.01 cm^3 cm^{-3}, respectively. The lines represent SMC_{up}-HSM curves under different soil moisture content at lower compartment. The top and bottom curves represent field capacity and permanent wilting point at lower compartment, respectively. The right and left arrows point to the condition of homogeneous field capacity and permanent wilting point in root zone, respectively. (For interpretation of the references to colour in this figure legend, the reader is referred to the web version of this article.)

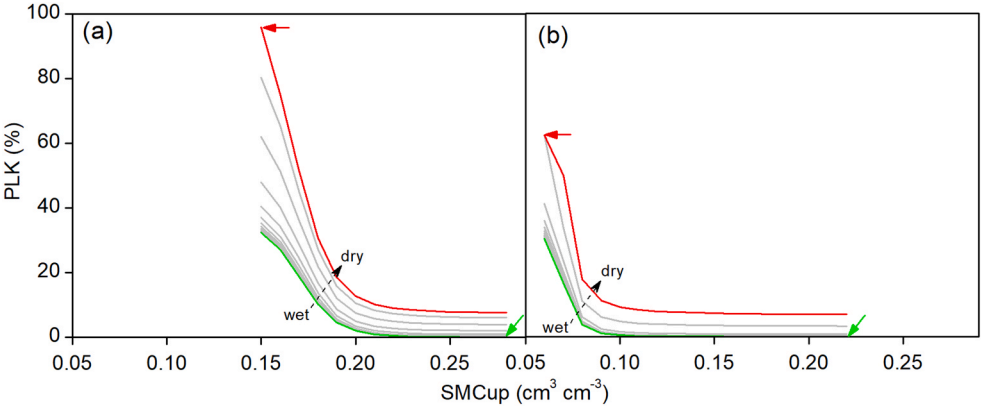

Fig. 8. Responses of percentage loss of soil-plant hydraulic conductance (PLK) to root-zone vertical soil moisture heterogeneity. Soil moisture contents at upper compartment (SMC_{up}) and lower compartment were in the range of permanent wilting point and field capacity, which was 0.15–0.28 cm^3 cm^{-3} for loamy clay (a) and 0.06–0.22 cm^3 cm^{-3} for sandy loam (b) at the interval of 0.01 cm^3 cm^{-3}, respectively. The lines represent SMC_{up}-PLK curves under different soil moisture content at lower compartment. The left and right curves represent field capacity and permanent wilting point at lower compartment, respectively. The bottom and top arrows point to the condition of homogeneous field capacity and permanent wilting point in root zone, respectively.

It ranged between 0.221 and 0.229 cm^3 cm^{-3} for loamy clay and 0.115–0.120 cm^3 cm^{-3} for sandy loam, respectively. The maximum value decreased from 3.26 to 2.22 mmol m^{-2} s^{-1}, and the minimum value decreased from 1.00 to 0.01 mmol m^{-2} s^{-1} with decreasing SMC_{down} in the two soil types.

3.2.2. *Change of the E_{crit}-SMC_{up} curve with SMC_{down}*

The E_{crit}-SMC_{up} curve decreased with decreasing SMC_{down} in both soils and was not affected by VPD (Fig. 6). The threshold changed little, and E_{crit} decreased in a similar rate when SMC_{up} decreased below threshold among different curves. As SMC_{down} decreased from field capacity to permanent wilting point, the threshold of E_{crit}-SMC_{up} curve

ranged between 0.223 and 0.227 cm^3 cm^{-3} and 0.108–0.116 cm^3 cm^{-3} for loamy clay and sandy loam, respectively. The maximum value decreased from 5.31 to 3.91 mmol m^{-2} s^{-1}, and the minimum value decreased from 2.09 to 0.03 mmol m^{-2} s^{-1} in the two soil types when SMC_{down} decreasing from field capacity to permanent wilting point.

3.2.3. Change of the HSM-SMC_{up} curve with SMC_{down}

As affected by E and E_{crit}, the HSM-SMC_{up} curve dropped with decreasing SMC_{down} in both soil types, and the patterns were impacted by VPD (Fig. 7). Under low VPD, the threshold was similar among different curves. It ranged between 0.229 and 0.236 cm^3 cm^{-3} for loamy clay and 0.118–0.125 cm^3 cm^{-3} for sandy loam. As SMC_{down} decreased from field capacity to permanent wilting point, the maximum value decreased from 3.43 to 2.39 mmol m^{-2} s^{-1}, and the minimum value decreased from 0.91 to 0.02 mmol m^{-2} s^{-1} in the two soil types.

Under middle VPD, the threshold of the HSM-SMC_{up} curve decreased substantially from 0.243 to 0.216 cm^3 cm^{-3} with decreasing SMC_{down} for loamy clay and from 0.140 to 0.098 cm^3 cm^{-3} for sandy loam. The maximum values of the HSM-SMC_{up} curves decreased from 2.32 to 1.73 mmol m^{-2} s^{-1} in the two soil types as the SMC_{down} decreased. These values were lower compared to those under low VPD. Meanwhile, HSM dropped at higher rates when SMC_{up} decreased below the threshold under lower SMC_{down}, causing the minimum value decreased from 1.08 to 0.02 mmol m^{-2} s^{-1} in the two soil types.

Under high VPD, the threshold fluctuated around 0.212–0.226 cm^3 cm^{-3} in loamy clay and 0.098–0.110 cm^3 cm^{-3} in sandy loam. When SMC_{down} decreased from field capacity to permanent wilting point, the maximum value of the curve decreased from 2.05 to 1.73 mmol m^{-2} s^{-1}. HSM dropped faster when SMC_{up} decreased below the threshold, and the minimum value decreased from 1.08 to 0.02 mmol m^{-2} s^{-1} in the two soil types.

3.2.4. Change of the PLK-SMC_{up} curve with SMC_{down}

The PLK-SMC_{up} curve rose with decreasing SMC_{down} in both soil types (Fig. 8) without difference under different VPD. The threshold was similar under different SMC_{down}, with range between 0.201 and 0.202 cm^3 cm^{-3} in loamy clay and 0.061–0.065 cm^3 cm^{-3} in sandy loam. As SMC_{down} decreased from field capacity to permanent wilting point, the minimum value varied slightly (0%~8%). PLK increased faster when SMC_{up} dropped below the threshold, and the maximum value increased from 32% to 96% in the two soil types.

4. Discussion

Plant water use characteristics at different soil depths are drawing the attention of researchers around the world, with the increasing long-term observations of soil moisture in deep soil profiles and the development of isotopic tracing method (Adams et al., 2019; Evaristo et al., 2015; Rossatto et al., 2012; Xi et al., 2018a; Yang et al., 2015, 2017). On this basis, the functional differences in shallow and deep soil water for plants are becoming more evident (Ryel et al., 2008; Yang et al., 2017). Characterizing plant response to root-zone soil moisture heterogeneity is essential for better understanding soil water availability to plants (Puértolas et al., 2020). With the help of mechanistically based models, researchers are able to separate the influence of soil, plant, and atmospheric factors on plants, and quantitatively assess these factors' comprehensive effect, which are difficult to analyze with experiments (Huber et al., 2015; Jackson et al., 2000; Novak et al., 2005). Sperry model explicitly simulates water transport through SPAC using the physics of flow through soil and xylem, efficiently defines the response of plant water use to soil and atmospheric drought, and calculates a series of unmeasurable hydraulic traits that reflects water transport safety (Sperry et al., 2016; Tai et al., 2018). In this study, we calibrated Sperry model with the vertical spilt-root experiments and verified the predictive accuracy of Sperry model for simulating SPAC water transport. We further analyzed the effect of root-zone vertical soil moisture heterogeneity on water transport safety in SPAC under different soil and atmospheric conditions. These quantitative findings are helpful for understanding the functional difference in soil water at different depths and optimizing water management in plantation forest and other ecosystems.

HSM and PLK are important indicators that reflect water transport safety in SPAC (Sperry et al., 1998; Sperry and Love, 2015; Tai et al., 2017, 2018), both of which were strongly affected by the soil moisture content in the upper and lower compartments in root zone according to the numerical analysis. HSM decreased rapidly as SMC_{up} decreased below the threshold (Fig. 7), while PLK exhibited the opposite trend (Fig. 8), indicating that water transport safety was significantly reduced when SMC_{up} was lower than the threshold. The HSM-SMC_{up} curves descended and PLK-SMC_{up} curves elevated gradually with decreasing SMC_{down}. Notably, PLK increased faster and the SMC_{up} had a greater impact on HSM under lower SMC_{down}, suggesting that water transport safety would be more sensitive to the variation in shallow soil water with decreasing soil water in deep soil. This finding supported the concept proposed by Ryel et al. (2008).

The results also have important implications for deep soil water management for improving water transport safety in SPAC in plantation forests and other ecosystems. For instance, in shallow water table areas, the seasonal variation in water table depth can substantially influence the dependence of SPAC water transport safety on the shallow soil water (Rossatto et al., 2012; Tai et al., 2018). In areas with deep water table, such as Loess Plateau, SPAC water transport can be limited frequently due to the fluctuation in shallow soil water with serious soil desiccation below the infiltration depth. Furthermore, the growth decline and forest dying back induced by hydraulic dysfunction can happen easily, which has been observed in *R. pseudoacacia* plantations in Loess Plateau in the previous studies (Wang et al., 2008; Wei et al., 2018). In this case, the mitigation approaches include (1) reducing soil water consumption in both shallow and deep layers through pruning, thinning, and other methods (Ma et al., 2019; Wang et al., 2020), and (2) enhancing water storage in deep soil by methods such as rain collection and infiltration system (Song et al., 2017), etc. In addition, subsurface drip irrigation can be adopted for improving soil moisture content in deep soil in some irrigated plantations like orchards, nurseries, etc.

The response of water transport safety in SPAC to SMC_{up} and SMC_{down} was also affected by soil texture and atmospheric evaporative demand. Compared with in loamy clay, HSM and PLK were more sensitive to the variation in soil moisture content in sandy loam since soil water potential and hydraulic conductivity decreased faster with decreasing soil moisture content in coarser-textured soils (van Genuchten, 1980). In Loess Plateau, soil texture is coarser, and climate is drier in the northern and western areas (Wang et al., 2010). Therefore, water transport safety in SPAC would be more easily impacted by soil moisture fluctuation in upper and lower layers in *R. pseudoacacia* plantations. Additionally, the HSM-SMC_{up} curves were strongly affected by VPD. The HSM is defined as the difference between E_{crit} and actual E, in which E_{crit} is determined mainly by soil water condition (Sperry and Love, 2015), whereas E varied strongly with VPD (Fig. 5). Transpiration response to soil water availability has been widely examined using experiments and modeling studies. The result showed that E remained stable at first, and then decreased rapidly with decreasing soil moisture content (Wu et al., 2011b; Yan et al., 2017). The relationship between E and soil moisture content or soil water potential can be quantified with a linear-plateau or s-shaped function, and it is influenced by soil, plant and atmospheric factors (Wu et al., 2015). In this study, the variation in E with SMC_{up} exhibited similar patterns (Fig. 5). Additionally, there was an interaction between SMC_{up} and SMC_{down} in influencing E since the E-SMC_{up} curves gradually descended with decreasing SMC_{down}. Under higher VPD, the maximum value of E-SMC_{up} curve was higher while E decreased substantially at higher SMC_{up} threshold, indicating that E was more sensitive to the variation in soil moisture content in upper and lower compartments. With decreasing SMC_{down}, HSM decreased in a

similar speed under low VPD, while HSM decreased faster under middle and high VPD when SMC_{up} decreased below the threshold. This result suggested that the decrease in SMC_{down} has a greater impact on water transport safety in SPAC under middle and high VPD. Meanwhile, the threshold of E_{crit}-SMC_{up} and E-SMC_{up} curves were lower in coarser-textured soils, thus HSM-SMC_{up} curves have lower threshold and HSM decreased faster when SMC_{up} decreased below the threshold (Fig. 7). On the other hand, the numerical simulations showed that the response of PLK to soil moisture content was not affected by VPD. This finding was mainly attributed to the assumption in Sperry model that stomatal aperture is regulated based on PLK (Eq. 2). The assumption should be examined with more studies, especially for the species with complex interactions between hydraulic and chemical signals in regulating stomatal behavior (Huber et al., 2015; Torres-Ruiz et al., 2015).

5. Conclusion

Sperry model could efficiently simulate SPAC water transport in *R. pseudoacacia* under the condition of soil moisture heterogeneity, presenting as an important tool for analyzing the effect of root-zone soil moisture heterogeneity on water transport safety in SPAC. The numerical simulations indicated that water transport safety in SPAC became more sensitive to soil moisture in upper root zone with decreasing soil moisture in the lower root zone, and strongly affected by the soil type and atmospheric evaporative demand. The results highlighted the importance of deep soil water management for water transport safety in SPAC and encouraged further studies. Sperry model can be further adopted to analyze the effect of eco-physiological properties of roots, such as the hydraulic redistribution on the function of soil water at different depths. Besides, Sperry model could be integrated with other eco-physiological processes, including carbon assimilation, plant growth, leaf shedding, etc. to analyze more physiological functions in response to root-zone soil moisture heterogeneity. More control experiments, especially the comparison between homogeneous and heterogeneous soil moisture treatments in both short and long-term experiments, should be conducted in further studies for better understanding the effect of soil moisture heterogeneity on water transport safety in SPAC.

Declaration of Competing Interest

The authors declare that they have no conflict of interest.

Acknowledgements

This research was financially supported by the Strategic Priority Research Program of Chinese Academy of Sciences (No. XDB40000000) and the National Natural Science Foundation of China (No. 41571213). The authors thank the members of the Changwu Ecology Station, Chinese Academy of Sciences, and Ministry of Water Resources for their assistance. We are very grateful to Professor John Sperry (University of Utah) for freely providing the plant hydraulic model.

Appendix A. Supporting information

Supplementary data associated with this article can be found in the online version at doi:10.1016/j.agwat.2020.106702.

References

Adams, M.A., Buckley, T.N., Turnbull, T.L., 2019. Rainfall drives variation in rates of change in intrinsic water use efficiency of tropical forests. Nat. Commun. 10, 3661.
Bauerle, T.L., Richards, J.H., Smart, D.R., Eissenstat, D.M., 2008. Importance of internal hydraulic redistribution for prolonging the lifespan of roots in dry soil. Plant, Cell Environ. 31, 177–186.
Caldwell, M.M., Dawson, T.E., Richards, J.H., 1998. Hydraulic lift: consequences of water efflux from the roots of plants. Oecologia 113, 151–161.
Chen, H.S., Shao, M.G., Li, Y.Y., 2008. Soil desiccation in the Loess Plateau of China. Geoderma 143, 91–100.
Choat, B., Brodribb, T.J., Brodersen, C.R., Duursma, R.A., Lopez, R., Medlyn, B.E., 2018. Triggers of tree mortality under drought. Nature 558, 531–539.
Damour, G., Simonneau, T., Cochard, H., Urban, L., 2010. An overview of models of stomatal conductance at the leaf level. Plant Cell Environ. 33, 1419–1438.
Domec, J.C., Warren, J.M., Meinzer, F.C., Brooks, J.R., Coulombe, R., 2004. Native root xylem embolism and stomatal closure in stands of Douglas-fir and ponderosa pine: mitigation by hydraulic redistribution. Oecologia 141, 7–16.
Domec, J.C., King, J.S., Noormets, A., Treasure, E., Gavazzi, M.J., Sun, G., McNulty, S.G., 2010. Hydraulic redistribution of soil water by roots affects whole-stand evapotranspiration and net ecosystem carbon exchange. N. Phytol. 187, 171–183.
Evaristo, J., Jasechko, S., McDonnell, J.J., 2015. Global separation of plant transpiration from groundwater and streamflow. Nature 525, 91–94.
Fan, Y., Miguez-Macho, G., Jobbágy, E.G., Jackson, R.B., Otero-Casal, C., 2017. Hydrologic regulation of plant rooting depth. PNAS 114, 10572–10577.
Feddes, R.A., Kowalik, P.J., Zaradny, H., 1978. Simulation of Field Water Use and Crop Yield. Pudoc, Wageningen.
Gaines, K.P., Stanley, J.W., Meinzer, F.C., McCulloh, K.A., Woodruff, D.R., Chen, W., Adams, T.S., Lin, H., Eissenstat, D.M., 2016. Reliance on shallow soil water in a mixed-hardwood forest in central Pennsylvania. Tree Physiol. 36, 444–458.
Gharsallah, O., Facchi, A., Gandolfi, C., 2013. Comparison of six evapotranspiration models for a surface irrigated maize agro-ecosystem in Northern Italy. Agric. Water Manag. 130, 119–130.
Hanks, R.J., Holmes, W.E., Tanner, C.B., 1954. Field capacity approximation based on the moisture-transmitting properties of the soil. Soil Sci. Soc. Am. J. 18, 252–254.
Hu, W., Shao, M.G., Han, F.P., Reichardt, K., 2011. Spatio-temporal variability behavior of land surface soil water content in shrub- and grass-land. Geoderma 162, 260–272.
Huber, K., Vanderborght, J., Javaux, M., Vereecken, H., 2015. Simulating transpiration and leaf water relations in response to heterogeneous soil moisture and different stomatal control mechanisms. Plant Soil 394, 109–126.
Jackson, R.B., Sperry, J.S., Dawson, T.E., 2000. Root water uptake and transport: using physiological processes in global predictions. Trends Plant Sci. 5, 482–488.
Jia, X., Zhao, C., Wang, Y., Zhu, Y., Wei, X., Shao, Ma, 2020. Traditional dry soil layer index method overestimates soil desiccation severity following conversion of cropland into forest and grassland on China's Loess Plateau. Agric. Ecosyst. Environ. 291, 106794.
Jia, X.X., Shao, M.A., Zhang, C.C., Zhao, C.L., 2016. Variation and simulation of soil water content within different soil depths along the south-north transect of the Loess Plateau. Adv. Water Sci. 27, 520–528.
Jia, X.X., Shao, M.A., Zhu, Y.J., Luo, Y., 2017. Soil moisture decline due to afforestation across the Loess Plateau, China. J. Hydrol. 546, 113–122.
Jia, Y.H., Li, T.C., Shao, M.A., Hao, J.H., Wang, Y.Q., Jia, X.X., Zeng, C., Fu, X.L., Liu, B. X., Gan, M., Zhao, M.Y., Ju, X.N., 2019. Disentangling the formation and evolvement mechanism of plants-induced dried soil layers on China's Loess Plateau. Agric. For. Meteorol. 269, 57–70.
Li, G.Q., Zhang, X.Q., Huang, J.H., Wen, Z.M., Du, S., 2018. Afforestation and climatic niche dynamics of black locust (Robinia pseudoacacia). For. Ecol. Manag. 407, 184–190.
Ma, C.K., Luo, Y., Shao, M.G., Li, X.D., Sun, L., Jia, X.X., 2017. Environmental controls on sap flow in black locust forest in Loess Plateau, China. Sci. Rep. 7, 13160.
Ma, L.H., Liu, X.L., Wang, Y.K., Wu, P.T., 2013. Effects of drip irrigation on deep root distribution, rooting depth, and soil water profile of jujube in a semiarid region. Plant Soil 373, 995–1006.
Ma, L.H., Wang, X., Gao, Z.Y., Wang, Y.K., Nie, Z.Y., Liu, X.L., 2019. Canopy pruning as a strategy for saving water in a dry land jujube plantation in a loess hilly region of China. Agric. Water Manag. 216, 436–443.
Nelder, J.A., Mead, R., 1965. A simplex method for function minimization. Comput. J. 7, 308–313.
Neumann, R.B., Cardon, Z.G., 2012. The magnitude of hydraulic redistribution by plant roots: a review and synthesis of empirical and modeling studies. N. Phytol. 194, 337–352.
Novak, V., Hurtalova, T., Matejka, F., 2005. Predicting the effects of soil water content and soil water potential on transpiration of maize. Agric. Water Manag. 76, 211–223.
Prieto, I., Armas, C., Pugnaire, F.I., 2012. Water release through plant roots: new insights into its consequences at the plant and ecosystem level. N. Phytol. 193, 830–841.
Puértolas, J., Pardos, M., de Ollas, C., Albacete, A., Dodd, I.C., 2020. Soil moisture heterogeneity regulates water use in Populus nigra L. by altering root and xylem sap phytohormone concentrations. Tree Physiol. 40, 762–773.
Reich, P.B., Sendall, K.M., Stefanski, A., Rich, R.L., Hobbie, S.E., Montgomery, R.A., 2018. Effects of climate warming on photosynthesis in boreal tree species depend on soil moisture. Nature 562, 263–267.
Rossatto, D.R., Silva, L.D.R., Villalobos-Vega, R., Sternberg, L.D.L., Franco, A.C., 2012. Depth of water uptake in woody plants relates to groundwater level and vegetation structure along a topographic gradient in a neotropical savanna. Environ. Exp. Bot. 77, 259–266.
Ryel, R., Ivans, C., Peek, M., Leffler, A.J., 2008. Functional Differences in Soil Water Pools: A New Perspective on Plant Water Use in Water-limited Ecosystems. Springer, Berlin, Heidelberg.
Schenk, H.J., 2005. Vertical vegetation structure below ground: scaling from root to globe. In: Esser, K., Lüttge, U., Beyschlag, W., Murata, J.E. (Eds.), Progress in Botany. Springer, Berlin, pp. 341–373.
Shangguan, Z.P., 2007. Soil desiccation occurrence an its impact on forest vegetation in the Loess Plateau of China. Int. J. Sustain. Dev. World Ecol. 14, 299–306.
Shao, M.A., Jia, X.X., Wang, Y.Q., Zhu, Y.J., 2016. A review of studies on dried soil layers in the Loess Plateau. Adv. Earth Sci. 31, 14–22.

Shu, L.Z., Liu, R., Min, W., Wang, Y.S., Hong-mei, Y., Zhu, P.F., Zhu, J.R., 2020. Regulation of soil water threshold on tomato plant growth and fruit quality under alternate partial root-zone drip irrigation. Agric. Water Manag. 238, 106200.
Song, X.L., Gao, X.D., Zhao, X.N., Wu, P.T., Dyck, M., 2017. Spatial distribution of soil moisture and fine roots in rain-fed apple orchards employing a Rainwater Collection and Infiltration (RWCI) system on the Loess Plateau of China. Agric. Water Manag. 184, 170–177.
Sperry, J.S., Love, D.M., 2015. What plant hydraulics can tell us about responses to climate-change droughts. N. Phytol. 207, 14–27.
Sperry, J.S., Donnelly, J.R., Tyree, M.T., 1988. A method for measuring hydraulic conductivity and embolism in xylem. Plant Cell Environ. 11, 35–40.
Sperry, J.S., Adler, F.R., Campbell, G.S., Comstock, J.P., 1998. Limitation of plant water use by rhizosphere and xylem conductance: results from a model. Plant Cell Environ. 21, 347–359.
Sperry, J.S., Stiller, V., Hacke, U.G., 2003. Xylem hydraulics and the soil-plant-atmosphere continuum: opportunities and unresolved issues. Agron. J. 95, 1362–1370.
Sperry, J.S., Wang, Y.J., Wolfe, B.T., Mackay, D.S., Anderegg, W.R.L., McDowell, N.G., Pockman, W.T., 2016. Pragmatic hydraulic theory predicts stomatal responses to climatic water deficits. New Phytol. 212, 577–589.
Tai, X.N., Mackay, D.S., Anderegg, W.R.L., Sperry, J.S., Brooks, P.D., 2017. Plant hydraulics improves and topography mediates prediction of aspen mortality in southwestern USA. New Phytol. 213, 113–127.
Tai, X.N., Mackay, D.S., Sperry, J.S., Brooks, P., Anderegg, W.R.L., Flanagan, L.B., Rood, S.B., Hopkinson, C., 2018. Distributed plant hydraulic and hydrological modeling to understand the susceptibility of riparian woodland trees to drought-induced mortality. Water Resour. Res. 54, 4901–4915.
Takahashi, F., Suzuki, T., Osakabe, Y., Betsuyaku, S., Kondo, Y., Dohmae, N., Fukuda, H., Yamaguchi-Shinozaki, K., Shinozaki, K., 2018. A small peptide modulates stomatal control via abscisic acid in long-distance signalling. Nature 556, 235–238.
Torres-Ruiz, J.M., Diaz-Espejo, A., Perez-Martin, A., Hernandez-Santana, V., 2015. Role of hydraulic and chemical signals in leaves, stems and roots in the stomatal behaviour of olive trees under water stress and recovery conditions. Tree Physiol. 35, 415–424.
van Genuchten, M.T., 1980. A closed-form equation for predicting the hydraulic conductivity of unsaturated soils. Soil Sci. Soc. Am. J. 44, 892–898.
van Genuchten, M.T., 1992. The RETC Code for Quantifying the Hydraulic Functions of Unsaturated Soils. U.S. Environmental Protection Agency, Robert S. Kerr Environmental Research Laboratory, Ada, OK.
Wang, L., Wang, Q., Wei, S., Shao, Ma, Li, Y., 2008. Soil desiccation for Loess soils on natural and regrown areas. For. Ecol. Manag. 255, 2467–2477.
Wang, R.Q., Zhang, L.L., Zhang, S.X., Cai, J., Tyree, M.T., 2014. Water relations of Robinia pseudoacacia L.: do vessels cavitate and refill diurnally or are R-shaped curves invalid in Robinia? Plant Cell Environ. 37, 2667–2678.
Wang, Y.Q., Shao, M.A., Liu, Z.P., 2010. Large-scale spatial variability of dried soil layers and related factors across the entire Loess Plateau of China. Geoderma 159, 99–108.
Wang, Y.Q., Shao, M.A., Zhu, Y.J., Liu, Z.P., 2011. Impacts of land use and plant characteristics on dried soil layers in different climatic regions on the Loess Plateau of China. Agric. For. Meteorol. 151, 437–448.
Wang, Y.Q., Shao, M.A., Liu, Z.P., 2013. Vertical distribution and influencing factors of soil water content within 21-m profile on the Chinese Loess Plateau. Geoderma 193, 300–310.
Wang, Y.Q., Shao, M.A., Sun, H., Fu, Z.H., Fan, J., Hu, W., Fang, L.C., 2020. Response of deep soil drought to precipitation, land use and topography across a semiarid watershed. Agric. For. Meteorol. 282–283, 107866.
Wei, J.S., Li, Z.S., Feng, X.Y., Zhang, Y., Chen, W.L., Xing, W.U., Jiao, L., Wang, X.C., 2018. Ecological and physiological mechanisms of growth decline of Robinia pseudoacacia plantations in the Loess Plateau of China: a review. Chin. J. Appl. Ecol. 29, 2433–2444.
Wolfe, B.T., Sperry, J.S., Kursar, T.A., 2016. Does leaf shedding protect stems from cavitation during seasonal droughts? A test of the hydraulic fuse hypothesis. N. Phytol. 212, 1007–1018.
Wu, Y.Z., Huang, M.B., Gallichand, J., 2011a. Transpirational response to water availability for winter wheat as affected by soil textures. Agric. Water Manag. 98, 569–576.
Wu, Y.Z., Huang, M.B., Warrington, D.N., 2011b. Growth and transpiration of maize and winter wheat in response to water deficits in pots and plots. Environ. Exp. Bot. 71, 65–71.
Wu, Y.Z., Huang, M.B., Warrington, D.N., 2011c. Responses of different physiological indices for maize (Zea mays) to soil water availability. Pedosphere 21, 639–649.
Wu, Y.Z., Huang, M.B., Warrington, D.N., 2015. Black locust transpiration responses to soil water availability as affected by meteorological factors and soil texture. Pedosphere 25, 57–71.
Xi, B.Y., Wang, Y., Jia, L.M., Bloomberg, M., Li, G.D., Di, N., 2013. Characteristics of fine root system and water uptake in a triploid Populus tomentosa plantation in the North China Plain: Implications for irrigation water management. Agric. Water Manag. 117, 83–92.
Xi, B.Y., Bloomberg, M., Watt, M.S., Wang, Y., Jia, L.M., 2016. Modeling growth response to soil water availability simulated by HYDRUS for a mature triploid Populus tomentosa plantation located on the North China Plain. Agric. Water Manag. 176, 243–254.
Xi, B.Y., Di, N., Cao, Z.G., Liu, J.Q., Li, D.D., Wang, Y., Li, G.D., Duan, J., Jia, L.M., Zhang, R.N., 2018a. Characteristics and underlying mechanisms of plant deep soil water uptake and utilization: implication for the cultivation of plantation trees. Chin. J. Plant Ecol. 42, 885–905.
Xi, B.Y., Di, N., Liu, J.Q., Zhang, R.N., Cao, Z.G., 2018b. Hydrologic regulation of plant rooting depth: pay attention to the widespread scenario with intense seasonal groundwater table fluctuation. Proc. Natl. Acad. Sci. 115, E3863–E3864.
Yan, W.M., Zhong, Y.Q.W., Shangguan, Z.P., 2017. Responses of different physiological parameter thresholds to soil water availability in four plant species during prolonged drought. Agric. For. Meteorol. 247, 311–319.
Yang, B., Wen, X.F., Sun, X.M., 2015. Seasonal variations in depth of water uptake for a subtropical coniferous plantation subjected to drought in an East Asian monsoon region. Agric. For. Meteorol. 201, 218–228.
Yang, F.T., Feng, Z.M., Wang, H.M., Dai, X.Q., Fu, X.L., 2017. Deep soil water extraction helps to drought avoidance but shallow soil water uptake during dry season controls the inter-annual variation in tree growth in four subtropical plantations. Agric. For. Meteorol. 234–235, 106–114.
Zhang, Z.D., Huang, M.B., Zhang, Y.K., 2018. Vertical distribution of fine-root area in relation to stand age and environmental factors in black locust (Robinia pseudoacacia) forests of the Chinese Loess Plateau. Can. J. For. Res. 48, 1148–1158.
Zhang, Z.D., Huang, M.B., Zhao, X.F., Wu, L.H., 2019. Adjustments of leaf traits and whole plant leaf area for balancing water supply and demand in Robinia pseudoacacia under different precipitation conditions on the Loess Plateau. Agric. For. Meteorol. 279, 107733.
Zhang, Z.D., Huang, M.B., Yang, Y.N., Zhao, X.F., 2020. Evaluating drought-induced mortality risk for Robinia pseudoacacia plantations along the precipitation gradient on the Chinese Loess Plateau. Agric. For. Meteorol. 284, 107897.
Zhou, S.X., Medlyn, B.E., Prentice, I.C., 2016. Long-term water stress leads to acclimation of drought sensitivity of photosynthetic capacity in xeric but not riparian Eucalyptus species. Ann. Bot. 117, 133–144.